Desalination and Water Treatment
www.deswater.com

14 (2010) 146–157
February

1944-3994/1944-3986
doi: 10.5004/dwt.2010.1020

Theoretical studies on carbon dioxide removal from a gas stream in hollow fiber membrane contactors

Noureddine Boucif[ab]*, Phuc Tien Nguyen[a], Denis Roizard[a], Eric Favre[a]

[a]*Laboratory of Reactions and enGineering Processes (LRGP) (UPR 6811-Nancy Université), ENSIC-BP 451 1, rue Grandville, F-54001 Nancy Cedex, France*
[b]*Département de Chimie Industrielle et LPQ3M, Faculté des Sciences de l'ingénieur, Université de Mascara, Mascara 29000, Algeria*
Tel. +33 3 83 17 53 90; Fax ++33 3 83 32 29 75; email: Noureddine.Boucif@ensic.inpl-nancy.fr

Received 24 June 2009; accepted 15 November 2009

ABSTRACT

This paper presents theoretical studies and modeling investigations on the reactive absorption of carbon dioxide in alkanolamine solutions, specially the monoethanolamine, in a hollow fiber membrane contactor device. The absorption mechanism was built based on mass transport conservation laws in all three regions involved in the process, i.e. the gas phase, the membrane barrier and the liquid region. The gas is flown in the fiber bore in which the velocity is assumed to obey a fully developed laminar flow, and the liquid solution is circulated counter-currently to the gas flow in the shell side where the velocity is characterized by the Happel's free surface model. The rigorous model consisting of a set of highly non-linear partial differential equations is rewritten in dimensionless form and numerically solved. The outlet gas and liquid concentrations are parametrically simulated with the gas and liquid flowrates (Graetz numbers) as well as inlet fresh solvent concentrations.

Keywords: Carbon dioxide removal; Hollow fibre membrane; Reactive absorption; Numerical simulation

1. Introduction

It has been proven that, among greenhouse gases, carbon dioxide, although a non-toxic gas, is the largest contributor in terms of emissions. The carbon dioxide concentrations will certainly continue to increase in the future as a result of fossil fuels combustion in the fields of transport, power production and heating. The human being high dependence on fossil fuels as energy generators and the tremendous difficulties in their replacement by alternative sustainable and renewable energies constrains us to search for and develop new techniques to reduce the polluting gases emitted by fossil fuel combustion especially carbon dioxide.

The reasons for removing CO_2 are usually of both technical and economical concerns. The carbon dioxide is generated in tremendous quantities by many important industries such as chemical and petrochemical industry, fossil fuel fired power plants, steel industry, cement production facilities, as well as natural gas treatment and liquefaction. The heating value of the natural gas is negatively affected by the carbon dioxide present in it. Besides, because of its acidity, the carbon dioxide causes harmful corrosion in pipes and process equipment, and acts as a catalyst poisoning in the ammonia synthesis process [1]. However, environmental

*Corresponding author

Presented at the Fourth Membrane Science and Technology Conference of Visegrad Countries (PERMEA 2009), Prague, 7-11 June, 2009.

concerns, such as global climate change, are now focused as one of the most important and challenging environmental issues facing the world community and have motivated intensive research on CO_2 capture and sequestration.

Capturing carbon dioxide from industrial gas streams by aqueous alkanolamine solutions is the most cost-effective technology available today.

The chemical absorption in hollow fiber membrane modules (HFMM) is an emerging hybrid technology that involves absorption with chemical reaction. This technique is operated over a wide range of volumetric flow rates and concentration levels to allow the reduction of polluting gases. The noticeable advantages of the HFMM over conventional technologies are the physical size and weight reduction of the gas-liquid contacting module. In addition to their flexibility, modularity and energy efficiency, this process offers high selectivity and appreciable transport driving force even for low concentration levels. Furthermore, the HFMM offers a much larger contact area per unit volume than packed columns or tray towers, as it overcomes the disadvantages such as entrainment and flooding at high flowrates, and reduces foaming on operating ones.

These contactors have been extensively investigated by many researchers since the early 70's in a wide range of applications, including among other processes the blood oxygenation, the hydrogen sulphide odor control, the carbon dioxide removal [2–7].

In previous work, Boucif et al. [2] have numerically simulated the absorption of carbon dioxide by typical industrial amines in a membrane contactor where the absorbent was flowing in the fiber bore.

In the present work, a numerical analysis was carried out to investigate the absorption of carbon dioxide in a microporous hollow fiber membrane contactor in which the contaminated gas stream is flowing in the fiber bore, and the absorbent in the cartridge shell side. The microscopic theoretical model includes the second order reversible reactions of the soluble gas in the absorbent based on the two-step carbamate formation mechanism. The main objective of this work is to develop a comprehensive theoretical mass transfer model, which numerical solution allows the performance evaluation of the HFMM contactor for the CO_2 absorption. The paper focuses on the carbon dioxide chemical absorption in alkanolamine solutions as absorbent. Although some researchers (Karoor, Mavroudi) [8,9] reported in their results the effect of liquid flowrate on contactor performance in terms of gas flowrate, their theoretical models were not clearly set. Henceforth, in this paper the three regions involved in the mass transfer process are delimited, and microscopic mass balances are set for each one of them. Furthermore, the present study, where both liquid and gas streams are run continuously, attempts to compare the gas and liquid flowrates effects on the absorption efficiencies of the membrane contactor.

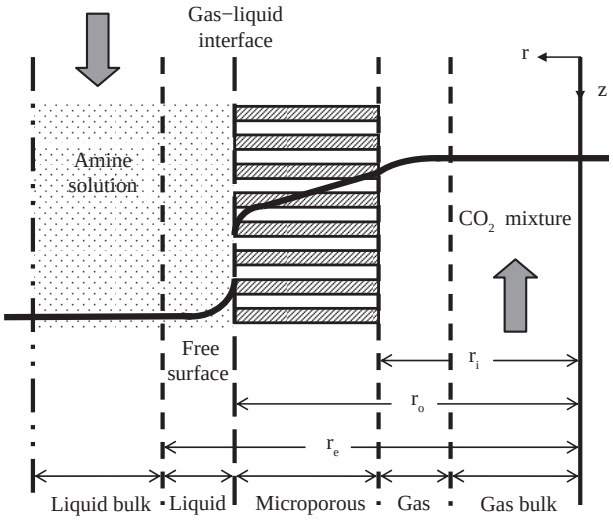

Fig. 1. Mass transfer domains and concentration profiles across in a HFMM contactor operated on a non-wetted mode.

2. Theory

In a contactor module with a hydrophobic microporous membrane, the absorption accompanied by a chemical reaction is a three step process as described in Fig. 1. The solute specie is transferred from the gas phase to the internal pore mouth of the membrane, then diffuses through the membrane's pores and finally absorbed by the solvent in the liquid solution where the reaction takes place.

As shown in Fig. 1, and based on the driving forces of the concentration differences, the molar mass transfer flux J_A of specie A is depicted as:

$$J_A = k_{Ag}\left(C_{Ag} - C^m_{Ag}\right) = k_{Am}\left(C^m_{Ag} - C^{int}_{Ag}\right) = k_{Al}\left(C^{int}_{Al} - C_{Al}\right) = K_{ov}\Delta C_A$$

Writing a component mass balance over the membrane module as drawn in Fig. 2, assuming no change in both gas and liquid flow rates, the inlet absorbent being a fresh amine solution, i.e. $[Am]_{in}$,

$$V[CO_2]_{in} - V[CO_2]_{out} = L[Am]_{out} \quad (1)$$

Besides, the right hand side of the above expression is merely the diffusion flux through the wall membrane which is calculated usually using the logarithmic mean concentration difference, as

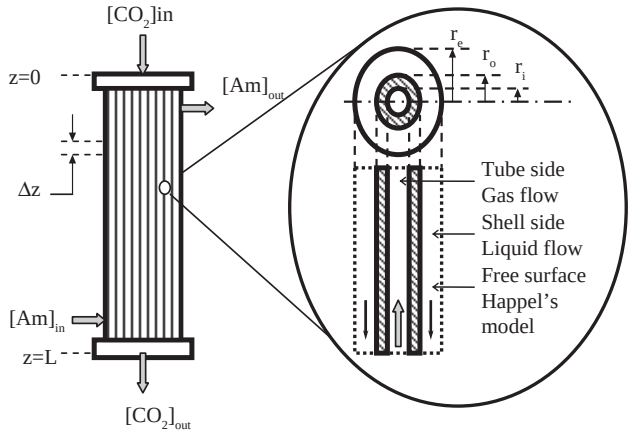

Fig. 2. Schematic diagram of an HFFM module and Happel's free surface model.

$$J = K_{ov} A_T \Delta C_{lm} \tag{2}$$

K_{ov}, the overall mass transfer coefficient, is usually related to the serial resistances against mass transfer in the three phases and calculated as:

$$\frac{1}{K_{ov}} = \frac{1}{k_{Ag}} + \frac{1}{k_{Am}} + \frac{1}{mEk_{Al}}$$

The gas and liquid phase mass transfer coefficients k_{Ag} and k_{Al} are determined by convection and diffusion respectively. The mass transfer resistance due to membrane is determined depending on the membrane structure and the molecular diffusion as detailed in [3].

The enhancement factor, E, expresses the effect of the chemical reaction on the absorption and is defined as the ratio of the chemically enhanced over the physical absorption fluxes at identical driving forces. The enhancement factor E is determined by de Coursey [10] as:

$$E = \frac{-Ha^2}{2(E_\infty^* - 1)} + \left[\frac{Ha^2}{4(E_\infty^* - 1)^2} + \frac{E_\infty^* Ha^2}{E_\infty^* - 1} + 1\right]^{1/2}$$

where Ha stands for the Hatta number and E_∞^* is the asymptotically infinite enhancement factor:

$$E_\infty^* = 1 + \frac{H[\mathrm{Am}]^{\mathrm{int}}}{H[\mathrm{CO_2}]^{\mathrm{int}}} \left[\frac{D_{\mathrm{Am}}}{D_{\mathrm{CO_2}}}\right]^{1/2}$$

For a reactive system of CO_2 with alkanolamines, Ha is expressed as:

$$Ha = \frac{\sqrt{k_{ov}[\mathrm{Am}]^{\mathrm{int}}\, D_{\mathrm{Am}}}}{k_{Al}}$$

The ΔC_{lm} is expressed, analogically to heat transfer [11] as:

$$\Delta C_{lm} = \frac{\left([\mathrm{CO_2}]_{out}^{int} - [\mathrm{Am}]_{in}\right) - \left([\mathrm{CO_2}]_{in}^{int} - [\mathrm{Am}]_{out}\right)}{\ln\left(\frac{[\mathrm{CO_2}]_{out}^{int} - [\mathrm{Am}]_{in}}{[\mathrm{CO_2}]_{in}^{int} - [\mathrm{Am}]_{out}}\right)} \tag{3}$$

with $[\mathrm{CO_2}]_{in}^{int}$ and $[\mathrm{CO_2}]_{out}^{int}$ being the concentrations of the solvent solution at the gas-liquid interface of the membrane wall. Introducing the Henry's law to estimate the liquid concentrations at the gas liquid interface, i.e. $[\mathrm{CO_2}]_{in}^{int} = H[\mathrm{CO_2}]_{in}$ and $[\mathrm{CO_2}]_{out}^{int} = H[\mathrm{CO_2}]_{out}$. After substitution and rearrangements we obtain then:

$$K_{ov} = \frac{L[\mathrm{Am}]_{out} \ln\left(\frac{H[\mathrm{CO_2}]_{out}}{H[\mathrm{CO_2}]_{in} - [\mathrm{Am}]_{out}}\right)}{A_T\{H[\mathrm{CO_2}]_{out} - (H[\mathrm{CO_2}]_{in} - [\mathrm{Am}]_{out})\}} \tag{4}$$

3. Mathematical Model Formulation

In previous papers [2,3], the liquid was flown inside the fiber bore and the gas velocity in the shell side was not taken into account. These shortcomings of these models could be overcome by considering the mass transfer process on either side of the membrane barrier. The mass transport is considered in all three domains involved in the transfer process, i.e. the fiber side, the membrane wall and the shell side of the module in which the gas and liquid concentrations are tied to each other at both fiber-inner wall and outer wall-shell frontiers by the appropriate boundary conditions.

The model considers the mass transport by convective diffusion of the gas first in the fiber bore (gas phase), then throughout the membrane's pores, and finally in the shell side (liquid phase) where a reaction with the absorbing solution is taking place. The basic concept of this model is schematically explained in Fig. 1. The main reason for circulating the gas inside the fiber bore and the liquid in the shell is simply because the gas is cleaner, and does not leave any deposit that will cause a hole fouling. Furthermore, this flow arrangement avoids excessive pressure drop of the viscous liquid.

3.1. Assumptions

The following assumptions are made to generate the governing equations of the CO_2 and the alkanolamine solution microscopic mass balances:

- The steady state process is isothermal and the gas mixture is assumed as an ideal gas

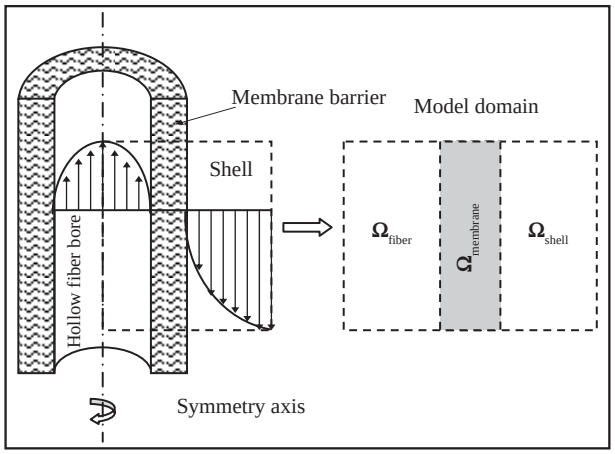

Fig. 3. Three domains hollow fiber membrane scheme.

- The axial diffusion is neglected in both tube and shell side
- The convective mass transfer in the gas-filled membrane's pores is neglected
- The absorbent liquid pressure drop in the shell side is neglected
- A fully developed concentration profiles is assumed in both fiber and shell sides
- Constant liquid absorbent viscosity and gas diffusivity in the liquid

3.2. Mass balances in the three areas

The module's hollow fiber membrane is split in three domains, as shown in Fig. 3, for each of which a transport material balance has been set up.

3.2.1. Fiber bore domain

In the fiber bore, the steady state CO_2 mass transfer by diffusion and convection is written as:

$$v_{zf} \cdot \nabla[CO_2]_f + \nabla \cdot \left[D_{CO_2-f} \nabla[CO_2]_f \right] = 0 \qquad (5)$$

If the gas velocity in the fiber bore is assumed to obey a fully developed parabolic profile, one can write:

$$v_{zf} = 2\bar{v}_{zf} \left[1 - \left(\frac{r}{r_i} \right)^2 \right] \qquad (6)$$

subject to the following initial and boundary conditions:

$$@ \quad z = 0, \quad [CO_2]_f = [CO_2]_{\text{initial}} = [CO_2]_{\text{in}} \quad \text{for any} \quad r_i \geq r \geq 0 \qquad (7)$$

$$@ \quad r = 0, \quad \frac{\partial [CO_2]_f}{\partial r} = 0 \quad \text{(for symmetry)} \quad \text{for any} \quad l \geq z \geq 0 \qquad (8)$$

$$@\ r = r_i, \quad [CO_2]_f = [CO_2]_m \quad \text{for any} \quad l \geq z \geq 0 \qquad (9)$$

3.2.2. Polymeric membrane domain

Through the membrane pores, the steady state CO_2 mass transfer is assumed to be mainly diffusive and written as:

$$\nabla \cdot \left[D_{CO_2-m} \nabla [CO_2]_m \right] = 0 \qquad (10)$$

subject to the following initial and boundary conditions:

$$@\ r = r_i, \ [CO_2]_m = [CO_2]_f \quad \text{for any} \quad l \geq z \geq 0 \qquad (11)$$

$$@\ r = r_o, \ [CO_2]_m = H[CO_2]_s \quad \text{for any} \quad l \geq z \geq 0 \qquad (12)$$

Furthermore, the carbon dioxide concentrations in the fiber side $[CO_2]_f$, in the membrane's pore $[CO_2]_m$ and in the shell side $[CO_2]_s$ are related to each other by the flux continuity equations at the fiber-membrane and at the membrane-shell boundaries as:

$$@\ r = r_i, \ D_{CO_2-f} \frac{\partial [CO_2]_f}{\partial r} = D_{CO_2-m} \frac{\partial [CO_2]_m}{\partial r} \qquad (13)$$

$$@\ r = r_o, \ D_{CO_2-m} \frac{\partial [CO_2]_m}{\partial r} = D_{CO_2-s} \frac{\partial [CO_2]_s}{\partial r} \qquad (14)$$

3.2.3. Shell domain

In the shell side, the steady state reactive absorbent mass transfer by diffusion and convection, the carbon dioxide reaction rate based on the two step carbamate formation model, is written for the gas and solvent respectively as:

$$\nu_{zs} \cdot \nabla [CO_2]_s + \nabla \cdot \left[D_{CO_2-S} \nabla [CO_2]_s \right] = R_{CO_2} \qquad (15)$$

$$v_{zs} \cdot \nabla [Am]_s + \nabla \cdot \left[D_{Am-s} \nabla [Am]_s \right] = R_{Am} \qquad (16)$$

The flow in the shell side of the membrane contactor, usually very complex, especially for a randomly distributed bundle of fibers, is characterized by the by the Happel's [12] free surface model represented in Figs. 1 and 2. This model, successfully used by Gill and Bansall [13], is given as:

$$v_{zs}(r) = 2\bar{v}_{zs}\left[1-\left(\frac{r_o}{r_e}\right)^2\right]\left\{\frac{\left(\frac{r}{r_e}\right)^2-\left(\frac{r_o}{r_e}\right)^2-\ln\left(\frac{r}{r_o}\right)^2}{3+\left(\frac{r_o}{r_e}\right)^4-4\left(\frac{r_o}{r_e}\right)^2+\ln\left(\frac{r_o}{r_e}\right)^4}\right\} \quad (17)$$

where r_e is the free surface radius and defined in terms of the packing fraction as: $r_e = \frac{r_s}{\sqrt{n_f}}$. The shell side volume fraction is easily obtained as: $\varepsilon = 1 - n_f\left[\frac{r_o}{r_s}\right]^2$.

A back substitution of the reaction rate and velocity yields:

$$2\bar{v}_{zs}\varepsilon\left[\frac{\varepsilon-1+(1-\varepsilon)\left(\frac{r}{r_o}\right)^2-\ln\left(\frac{r}{r_o}\right)^2}{\varepsilon(\varepsilon+2)+\ln(1-\varepsilon)^2}\right]\frac{\partial[\mathrm{Am}]_s}{\partial z} = D_{\mathrm{Am}-s}\left[\frac{\partial^2[\mathrm{Am}]_s}{\partial r^2}+\frac{1}{r}\frac{\partial[\mathrm{Am}]_s}{\partial r}\right]-R_{\mathrm{CO_2}}$$

R_{CO_2} stands for the carbon dioxide reaction rate in the liquid phase. The reaction rate is based on the two step carbamate formation mechanism.

$$R_{\mathrm{CO_2}} = \left(\frac{k_1}{1+\frac{k_{-1}}{k_B[\mathrm{Am}]_s}}\right)\left\{[\mathrm{CO_2}]_s[\mathrm{Am}]_s-\frac{(C_T-[\mathrm{Am}]_s)^2}{4K_{\mathrm{eq}}[\mathrm{Am}]_s}\right\} \quad (18)$$

In the case of MEA, the term $k_{\mathrm{am}}[\mathrm{Am}]$ is assumed very large compared to k_{-1} [14]. The reaction rate constant has been calculated from the expression $\log_{10}k_1 = 10.99 - \frac{2{,}152}{T(^\circ\mathrm{K})}$, derived by Hikita et al. [15] and valid in the range of 5–80°C, and 0.0152–0.177 kg mole/m^3 or in an Arrhenius form as $k_1 = A_R\exp\left[-\frac{E_R}{\Re T_l^0}\right]$, where the second order rate constant $A_R = 9.7744 \times 10^{10}$m^3/mol s, and the activation energy E_R = 41,197.53 J/mol.

The above differential equation is subject to the initial and boundary conditions:

$$@\ z = l,\ [\mathrm{Am}]_s = C_T \quad \text{and} \quad [\mathrm{CO_2}]_s = 0 \quad \text{for any} \quad r_i \geq r \geq 0 \quad (19)$$

$$@\ r = r_o,\ [\mathrm{CO_2}]_s = m[\mathrm{CO_2}]_m \quad \text{and} \quad \frac{\partial[Am]_s}{\partial r} = 0 \quad \text{for any} \quad l \geq z \geq 0 \quad (20)$$

$$@\ r = r_e,\ \frac{\partial[\mathrm{CO_2}]_s}{\partial r} = 0 \quad \text{and} \quad \frac{\partial[\mathrm{Am}]_s}{\partial r} = 0 \quad \text{for symmetry} \quad l \geq z \geq 0 \quad (21)$$

The outlet gas and solvent concentration, in the fiber bore and the shell respectively $[\mathrm{CO_2}]_f^{\mathrm{out}}$, $[\mathrm{CO_2}]_s^{\mathrm{out}}$ and $[\mathrm{Am}]_s^{\mathrm{out}}$ are determined as ''mixing cup'' concentrations, given by Skelland [16] as:

Table 1
Characteristics of the hollow fiber contactors used in this study

Characteristics	Module 2
Fibers material	Polypropylene (PP)
Polymer nature	Microporous
Fiber inner diameter (μm)	330
Fiber outer diameter (μm)	360
Thickness δ (μm)	15
Average pore size r_p (μm)	0.6
Porosity (ϵ)	0.4
Tortuosity ($\tau = (2-\varepsilon)^2/\varepsilon$)	6.4
Number of fibers	1,930
Active module length (mm)	200
Shell inner diameter (mm)	35
Inner contact area (m^2)	0.4
Outer contact area (m^2)	0.4363
Void fraction (ϕ)	0.204
Surface to volume fraction (m^2/m^3)	2,300

$$[\mathrm{CO_2}]_f^{\mathrm{out}} = \frac{\int_0^{r_i} 2\pi r v_{zf}(r)[\mathrm{CO_2}]_f \mathrm{d}r}{\int_0^{r_i} 2\pi r v_{zf}(r)\mathrm{d}r},$$

$$[\mathrm{CO_2}]_s^{\mathrm{out}} = \frac{\int_{r_o}^{r_e} 2\pi r v_{zs}(r)[\mathrm{CO_2}]_s\ \mathrm{d}r}{\int_{r_o}^{r_o} 2\pi r v_{zs}(r)\mathrm{d}r}$$

$$\text{and} \quad [\mathrm{Am}]_s^{\mathrm{out}} = \frac{\int_{r_o}^{r_e} 2\pi r v_{zs}(r)[\mathrm{Am}]_s\ \mathrm{d}r}{\int_{r_o}^{r_e} 2\pi r v_{zs}(r)\mathrm{d}r}$$

The model equations, rewritten in dimensionless form and listed in Appendix A, were solved using the direct linear system solver UMFPACK of COMSOL Multiphysics Modeling version 3.5, a very friendly used software package licensed from COMSOL Inc., Burlington, Massachusetts. COMSOL Multiphysics Modelling, a powerful computer software, uses the finite element method to solve fluid flow, mass and heat transport, as well as many other engineering problems. A comprehensive account of COMSOL Multiphysics Modeling is available in Zimmerman [17]. And very recently, an extensive overview of many of the choices provided by this software has been presented by Finlayson [18], by means of different illustrations on how to solve complicated problems.

4. Results and discussion

The absorption accompanied by chemical reaction in a microporous hollow fiber membrane contactor with the module characteristics summarized in Table 1 and the CO_2-MEA system physico-chemical properties listed in Table 2 is studied in this paper. The three

Table 2
Physico-chemical parameters of the CO_2-MEA chemical absorption at 298.14 °K

Designation	Symbol	Value	Reference
Reaction rate constant ($mol/m^3.s$)	k_1	$10^{(10.99-2152/T)}/1,000$	[10]
Equilibrium constant (mol/m^3)	K_{eq}	172.97	[10]
Partition coefficient (dimensionless)	$m = 1/H$	$(2.82 \times 10^{-6}/\Re T)\exp(-2,044/T)$	[20]
Diffusivity of CO_2 in the fiber (m^2/s)	$D_{CO_2\_f}$	1.855×10^{-5}	[19]
Diffusivity of CO_2 in the PP (m^2/s)	$D_{CO_2\_m}$	1.855×10^{-5} (ϵ/τ)	[Estimated]
Diffusivity of CO_2 in the shell (m^2/s)	$D_{CO_2\_s}$	$(2.35 \times 10^{-6}/RT)\exp(-2,199/T)$	[20]

dimensionless gas phase carbon dioxide concentration profiles are displayed and the gas and liquid flowrates, as well as fresh solvent concentration on gas and liquid phase solute and solvent are presented.

The solute concentration distribution is represented in Fig. 4 in all three domains of the contactor: the fiber bore, the membrane barrier and the shell side. The gas mixture is admitted to the fiber lumen of the contactor at its maximum solute concentration, whereas the solvent enters the module from the opposite side, and flows in a countercurrent flow pattern. Due to the difference in concentration, and as the gas stream flows through the fiber lumen, the solute is moving toward the membrane at the pore mouth of which it is absorbed by the moving solvent.

Fig. 5 presents the dimensionless radial concentration profile of the gas solute in the fiber, membrane and shell compartments of the hollow fiber contactor. It is observed that the solute concentration is almost constant in the fiber domain, and then it drastically decays when crossing the membrane barrier, and

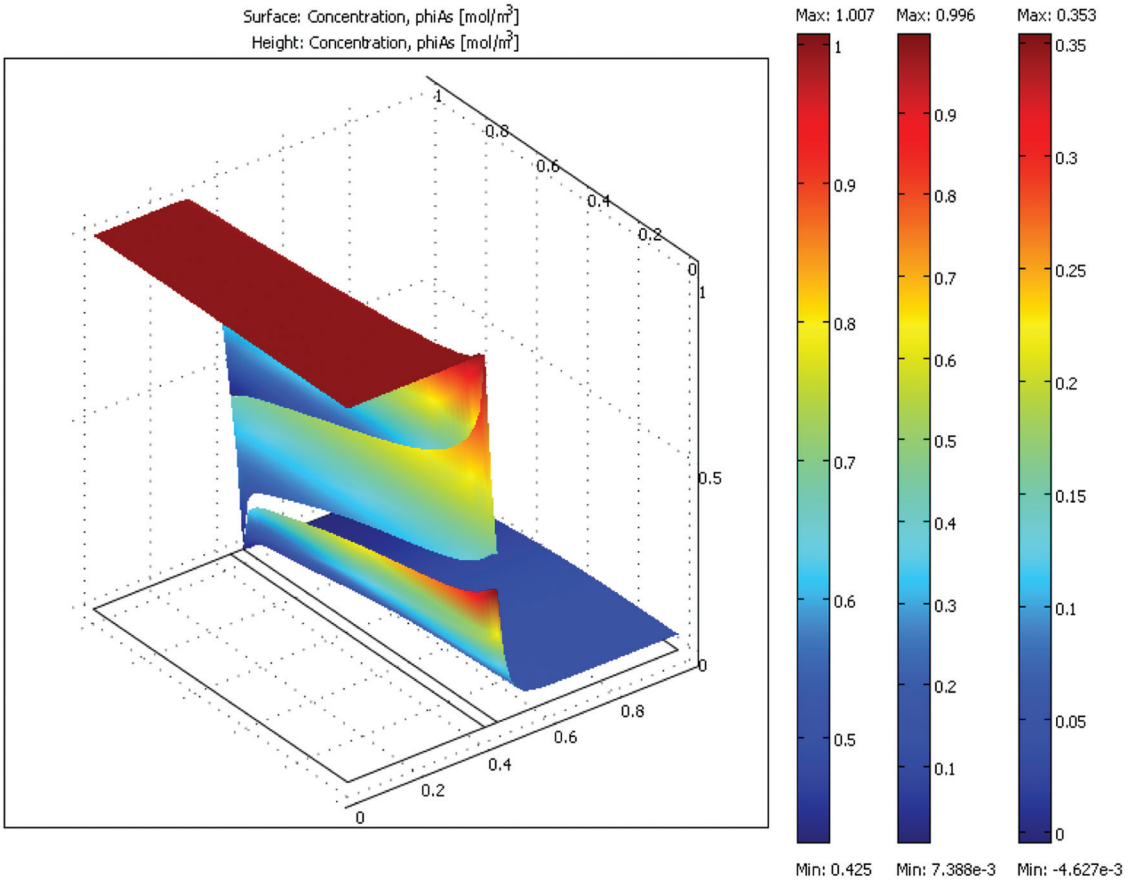

Fig. 4. 3D solute concentration profiles in all three domains ($[CO_2]_{in} = 5.0\ mol/m^3$ $C_T = 1,200\ mol/m^3$, $L = 100\ cm^3/mn$, $V = 10\ cm^3/mn$).

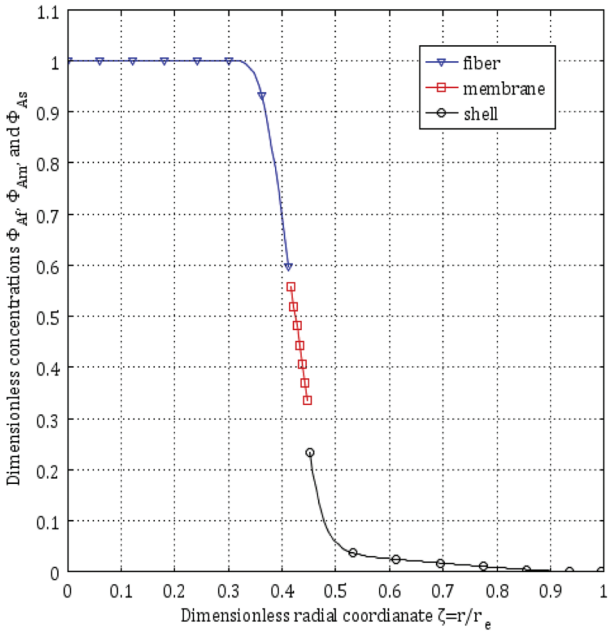

Fig. 5. Carbon dioxide concentration profiles in the radial direction ($[CO_2]_{in} = 5.0$ mol/m^3, $C_T = 1,200$ mol/m^3, $L = 100$ cm^3/mn, $V = 10$ cm^3/mn).

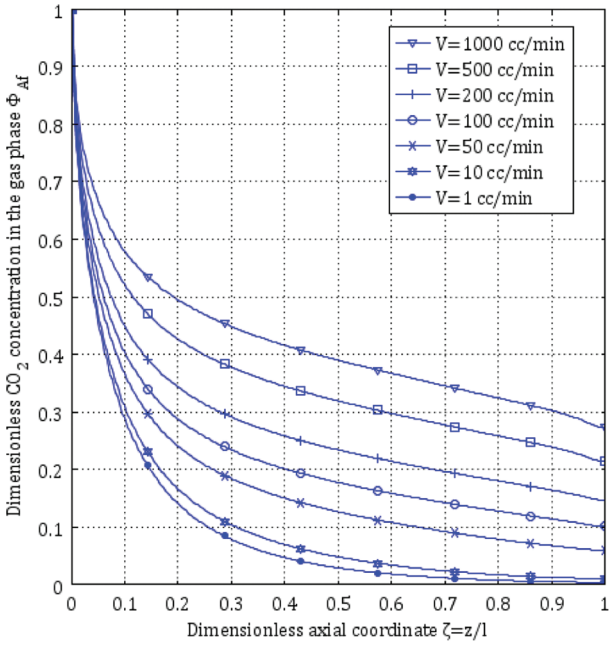

Fig. 6. Gas phase CO_2 concentration throughout the fiber at different gas flowrates V ($[CO_2]_{in} = 5.0$ mol/m^3, $C_T = 1,200$ mol/m^3, $L = 100$ cm^3/mn).

finally decreases smoothly in the shell side where the absorbent solution is moving. The reason of such behavior is that the solute diffusion coefficient in the fiber lumen is much higher than those in both the membrane and shell compartments. Consequently, the solute mass transfer encounters a much lower resistance in the gas phase within the fiber bore than those in the membrane and liquid phase flowing in the shell side.

Fig. 6 depicts dimensionless solute concentration in the gas phase throughout the length of the hollow fiber module at different gas flowrate values. It is clearly observed that the outlet dimensionless solute concentration ($\varsigma = 1$) in the gas stream is decreasing when the gas flowrates are gradually decreased, i.e. the solute removal rate is improving at higher residence times of the solute in the gas phase.

Conversely, as clearly shown in Fig. 7, the liquid flowrate has an opposite effect on this dimensionless solute concentration in the gas stream. When the liquid absorbent is moving slower in the shell side, the solute gas concentration at the outer surface of the fiber along the module length is increasing, resulting in a lower concentration gradient at the interface, therefore a poor removal rate (Fig. 8).

Fig. 9 exhibits the dimensionless solute concentration in the liquid phase along the fiber contactor at different liquid flowrates. It is observed from the figure that the outlet dimensionless solute concentration ($\varsigma = 0$) in the liquid absorbent is enriched when increasing the moving liquid flowrates in the shell compartment. However, the dimensionless outlet

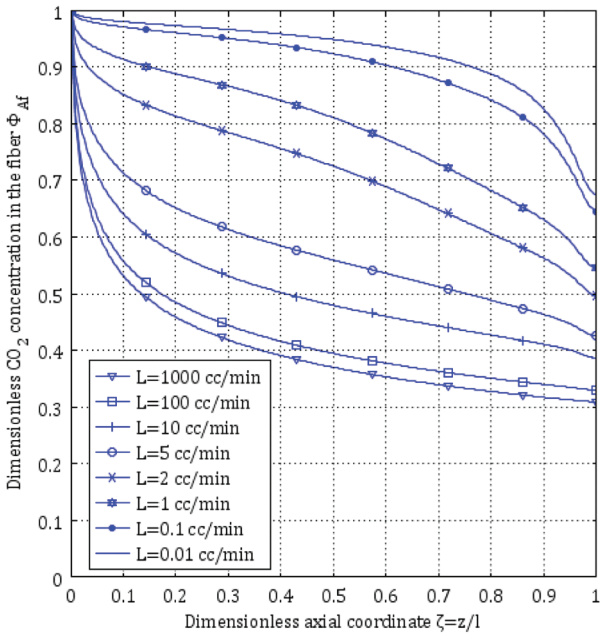

Fig. 7. Gas phase CO_2 concentration throughout the fiber at different liquid velocities L ($[CO_2]_{in} = 5.0$ mol/m^3, $C_T = 1,200$ mol/m^3, $V = 10$ cm^3/mn).

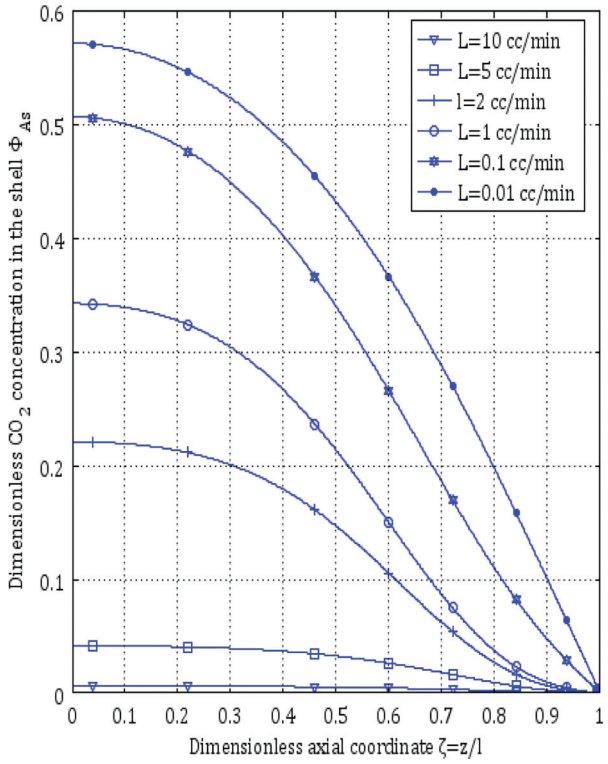

Fig. 8. Liquid phase CO_2 concentration throughout the shell at different liquid velocities L ($[CO_2]_{in} = 5.0$ mol/m^3, $C_T = 1,200$ mol/m^3, $V = 10$ cm^3/mn).

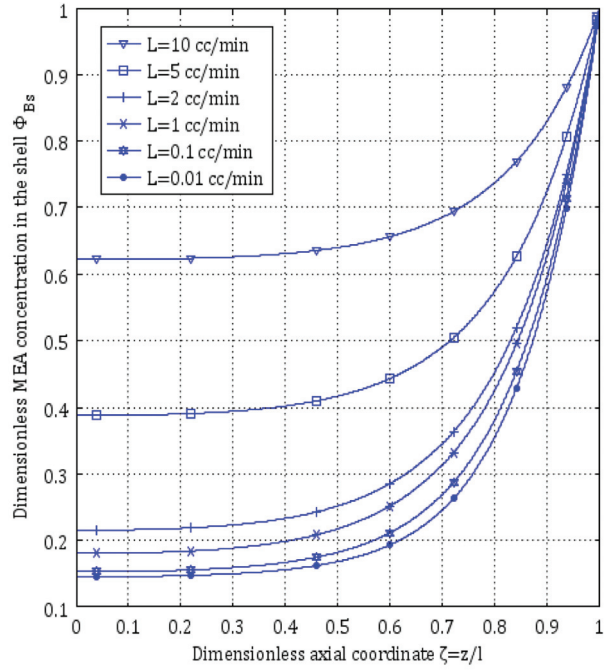

Fig. 9. Solvent MEA concentration throughout the shell at different liquid velocities L ($[CO_2]_{in} = 5.0$ mol/m^3, $C_T = 1,200$ mol/m^3, $V = 10$ cm^3/mn).

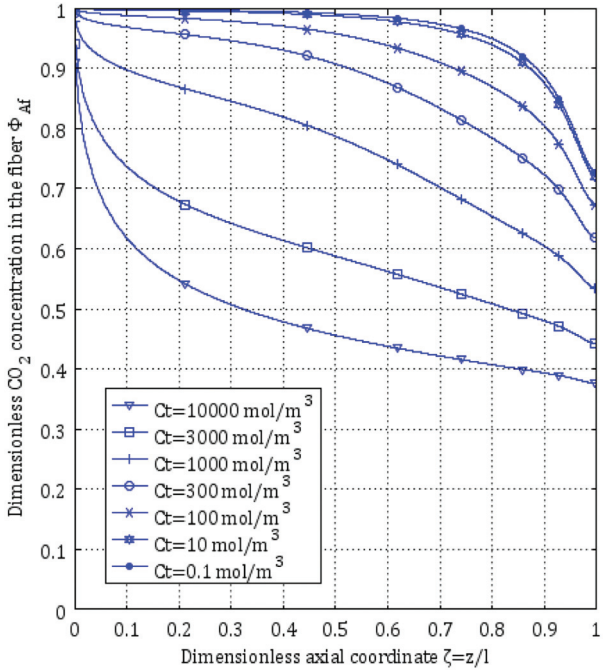

Fig. 10. Gas phase CO_2 concentration throughout the fiber at different fresh MEA concentrations C_T ($[CO_2]_{in} = 5.0$ mol/m^3, $L = 100$ cm^3/mn, $V = 10$ cm^3/mn).

solvent concentration is leaner for decreasing liquid absorbent flowrates, which implies an increased solute to solvent contact time, hence improving reactive absorption at the gas liquid interface. The effect of the inlet solvent concentration on the outlet solute concentration in the fiber bore is depicted by Fig. 10 which reveals that the gas phase carbon dioxide sequestration is favored by richer fresh amine solution.

5. Conclusion

A comprehensive momentum and mass transport mathematical model has been developed to simulate gas absorption accompanied by chemical reaction in hollow fiber membrane contactors. The dimensionless governing differential equations in all three contactor domains (fiber, membrane and shell) have been numerically solved and simulated over influencing process parameters.

The modeling results of the investigated system (carbon dioxide gas absorption in monoethanolamine as a solvent), indicate that the solute removal rate in the fiber is positively affected by increasing the liquid absorbent flowrate in the shell and decreasing the gas stream flowrate.

Symbols

A_T	total surface area of gas liquid contact (m^2)
C_T	total inlet solvent concentration (mol/m^3)
D_{CO_2-f}	diffusion coefficient of (CO_2) specie in the fiber side (m^2/s)
D_{CO_2-m}	diffusion coefficient of (CO_2) specie in the membrane (m^2/s)
D_{CO_2-s}	diffusion coefficient of (CO_2) specie in the shell side (m^2/s)
D_{CO_2-K}	continuum Knudsen diffusion coefficient of (CO_2) specie (m^2/s)
E	enhancement factor
Gr_{Af}	dimensionless Graetz number of specie A (CO_2) in the fiber side
Gr_{As}	dimensionless Graetz number of specie A (CO_2) in the shell side
Gr_{Bs}	dimensionless Graetz number of specie B (MEA) in the shell side
H	dimensionless Henry's law constant (–)
Ha	dimensionless Hatta number
J_A	molar mass transfer flux of specie A (mol/s)
k_{CO_2-f}	gas film mass transfer coefficient of A (CO_2) specie (m/s)
k_{CO_2-s}	liquid film mass transfer coefficient of A (CO_2) specie (m/s)
k_{CO_2-m}	membrane mass transfer coefficient of A (CO_2) specie (m/s)
k_{am}	forward second order reaction rate constant (m^3/mole.s)
k_1	forward second order reaction rate constant (m^3/mole.s)
k_{-1}	reverse second order reaction rate constant (m^3/mole.s)
k_{ov}	overall reaction constant
K_{eq}	equilibrium constant (–)
K_{ext}	external mass transfer coefficient (m/s)
K_{ov}	overall mass transfer coefficient (m/s)
L	liquid flow rate (m^3/s)
L	active membrane fiber length (m)
M	partition coefficient
M_A	solute molecular weight (kg/mol)
N	number of fiber in the bundle (–)
R	radial coordinate
r_i	inner fiber radius (m)
r_o	outer fiber radius (m)
r_e	free surface radius (m)
r_p	mean pore radius (m)
$\Re$	ideal gas constant (8.314 Pa m^3/mol K)
Sh_{Af}	dimensionless Sherwood number of specie A (CO_2) in the fiber (–)
Sh_{Am}	dimensionless Sherwood number of specie A (CO_2) in the membrane (–)
Sh_{As}	dimensionless Sherwood number of specie A (CO_2) in the shell side (–)
T	temperature in °K
V	gas flow rate (m^3/s)
$v_z(r)$	radius dependant velocity in the z direction
$\bar{v}_{zf}$	mean average velocity in the fiber in the z direction (m/s)
$\bar{v}_{zs}$	mean average velocity in the shell in the z direction (m/s)
z	axial contactor coordinate

Greek symbols

Φ_{Af}	dimensionless concentration of CO_2 in the fiber lumen
Φ_{Am}	dimensionless concentration of CO_2 in the gas gas-filled membrane pores
Φ_{As}	dimensionless concentration of CO_2 in the shell side
Φ_{Bs}	dimensionless concentration of the liquid absorbent in the shell side
ς	dimensionless longitudinal coordinate
ξ	dimensionless radial coordinate in the tube domain
ε	fiber bundle to shell packing fraction
ψ	extent of specie removal
δ	membrane thickness
τ	membrane's pore tortuosity

Subscripts

f	fiber
m	membrane
s	shell

References

[1] G.D. Astarita, W. Savage and A. Bisio, Gas Treating with Chemical Solvents, John Wiley and Sons, New York, 1983.

[2] N. Boucif, E. Favre and D. Roizard, CO_2 capture in HFMM contactor with typical amine solutions: a numerical analysis, Chem. Eng. Sci., 63 (2008) 5375–5385.

[3] N. Boucif, E. Favre, D. Roizard and M. Belloul, Hollow fiber membrane contactor for hydrogen sulfide odor control, AIChE J., 54 (2008) 122–131.

[4] E.L. Cussler, Diffusion Mass Transfer in Fluid Systems, Cambridge University Press, Cambridge, 1984.

[5] O. Falk-Pedersen and H. Dannstrom, Separation of carbon dioxide from offshore gas turbine exhaust, Energy Conv. Manage., 38 (1997) S81-S86.

[6] H.A. Rangwala, Absorption of carbon dioxide into aqueous solutions using hollow fiber membrane contactors, J. Membr. Sci., 112 (1996) 229–240.

[7] P.H.M. Feron and A.E. Jansen, CO_2 separation with polyolefin membrane contactors and dedicated absorption liquids: performance ands prospects, Sep. Purif. Technol., 27 (2002) 231–242.

[8] S. Karoor and K.K. Sirkar, Gas absorption studies in microporous hollow fiber membranes, Ind. Eng. Chem. Res., 32 (1993) 674–684.

[9] M. Mavroudi, S.P. Kaldis and G.P. Sakellaropoulos, Reduction of CO_2 emission by a membrane contacting process. Fuel, 82 (2003) 253–259.
[10] W.J. de Coursey, Enhancement factor for gas absorption with reversible chemical reaction, Chem. Eng. Sci., 37 (1982) 1483–1489.
[11] R.E. Treybal, Mass-Transfer Operations (3rd edn, reissue), McGraw-Hill, New York, 1987.
[12] J. Happel, Viscous flow relative to array of cylinders, AIChE J., 5 (1959) 174–177.
[13] W.N. Gill and B. Bansal, Hollow fiber reverse osmosis systems analysis and design, AIChE J., 19 (1973) 823–831.
[14] P.V. Danckwerts, The reactions of CO_2 with ethanolamines, Chem. Eng. Sci., 34 (1979) 443–446.
[15] H. Hikita, S. Asai, H. Ishikawa and M. Honda, The kinetics of reactions of carbon dioxide with diethanolamine and triethanolamine by a rapid mixing method, Chem. Eng. J., 13 (1977) 7–12.
[16] A.H.P. Skelland, Diffusional Mass Transfer, John Wiley and Sons, New York, 1974.
[17] W.B.J. Zimmerman, Process Modelling and Simulation with Finite Element Methods, World Scientific, Singapore, 2004.
[18] B.A. Finlayson, Introduction to Chemical Engineering Computing, John Wiley and Sons, New York, 2006.
[19] G.F. Versteeg and W.P.M. van Swaaij, Solubility and diffusivity of acid gases (CO2, N2O) in aqueous alkanolamine solutions, J. Chem. Eng. Data, 33 (1987) 29–34.
[20] K. Esato and B. Eisman, Experimental evaluations of Gore Tex™ membrane oxygenator, J. Thor. Cardiovasc. Surg., 69 (1975) 690–697.

Appendix A: Dimensionless Form of the Modeling Equations

Introducing the new independent and dependant variables:

$$\varsigma = \frac{z}{l}, \quad \xi = \frac{r}{r_e}, \quad \Phi_{\mathrm{Af}} = \frac{[\mathrm{CO_2}]_f}{[\mathrm{CO_2}]_{\mathrm{in}}}, \quad \Phi_{\mathrm{Am}} = \frac{[\mathrm{CO_2}]_m}{[\mathrm{CO_2}]_{\mathrm{in}}},$$
$$\Phi_{\mathrm{As}} = \frac{[\mathrm{CO_2}]_s}{[\mathrm{CO_2}]_{\mathrm{in}}}, \quad \Phi_{\mathrm{Bs}} = \frac{[\mathrm{Am}]_s}{C_T}$$

The mass transport governing equations in all three domains along with their corresponding initial and boundary conditions are rewritten in a dimensionless form.

1. Mass balance in the fiber bore

$$Gr_{\mathrm{Af}} \frac{(1-\xi^2)}{2} \frac{\partial \Phi_{\mathrm{Af}}}{\partial \varsigma} + \nabla \cdot [-\nabla \Phi_{\mathrm{Af}}] = 0 \tag{A1}$$

subject to the normalized initial and boundary conditions:

$$@\ \varsigma = 0, \quad \Phi_{\mathrm{Af}} = 1 \tag{A2}$$

$$@ \quad \xi = 0, \quad \left.\frac{\partial \Phi_{\mathrm{Af}}}{\partial \xi}\right|_{\xi=0} = 0 \tag{A3}$$

$$@\ \xi = \frac{r_i}{r_e} = \lambda_1, \quad \Phi_{\mathrm{Af}} = \Phi_{\mathrm{Am}} \tag{A4}$$

2. Mass balance through the membrane pore

$$\nabla \cdot [-\nabla \Phi_{\mathrm{Am}}] = 0 \tag{A5}$$

subject to the normalized boundary conditions:

$$@\ \xi = \frac{r_i}{r_e} = \lambda_1, \quad \Phi_{\mathrm{Am}} = \Phi_{\mathrm{Af}}, \quad \text{and} \quad \left.\frac{\partial \Phi_{\mathrm{Af}}}{\partial \xi}\right|_{\xi=\lambda_1} = \alpha_1 \left.\frac{\partial \Phi_{\mathrm{Am}}}{\partial \xi}\right|_{\xi=\lambda_2} \tag{A6}$$

$$@ \quad \xi = \frac{r_o}{r_e} = \lambda_2, \quad \Phi_{\mathrm{Am}} = H\Phi_{\mathrm{As}}, \quad \text{and} \quad \left.\frac{\partial \Phi_{\mathrm{Am}}}{\partial \xi}\right|_{\xi=\lambda_1} = \alpha_2 \left.\frac{\partial \Phi_{\mathrm{As}}}{\partial \xi}\right|_{\xi=\lambda_2} \tag{A7}$$

with $\alpha_1 = \frac{D_{\mathrm{CO_2}-m}}{D_{\mathrm{CO_2}-f}}$ and $\alpha_2 = \frac{D_{\mathrm{CO_2}-s}}{D_{\mathrm{CO_2}-m}}$

3. Mass balance in shell side

$$\frac{Gr_{\mathrm{As}}}{2p(\xi)} \frac{\partial \Phi_{As}}{\partial \varsigma} + \nabla \cdot [-\nabla \Phi_{\mathrm{As}}] = -\frac{\beta_1 Gr_{\mathrm{As}}}{4} \Omega_{\mathrm{CO_2}} \tag{A8}$$

$$\frac{Gr_{\mathrm{Bs}}}{2p(\xi)} \frac{\partial \Phi_{\mathrm{Bs}}}{\partial \varsigma} + \nabla \cdot [-\nabla \Phi_{\mathrm{Bs}}] = -\frac{\beta_2 Gr_{\mathrm{Bs}}}{2} \Omega_{\mathrm{CO_2}} \tag{A9}$$

where the involved variables and rate of reaction are determined as:

Table 3
Dimensionless groupings definition

Designation	Symbol	Expression
Graetz number of CO_2 in fiber side	Gr_{Af}	$\frac{\bar{v}_{zf} d_e^2}{l D_{\mathrm{CO_2}-g}}$
Graetz number of CO_2 in shell side	Gr_{As}	$\frac{\bar{v}_{zs} d_e^2}{l D_{\mathrm{CO_2}-\mathrm{Am}}}$
Graetz number of MEA in shell side	Gr_{Bs}	$\frac{\bar{v}_{zs} d_e^2}{l D_{\mathrm{Am}-w}}$
Reaction parameter of MEA in the fiber	β_1	$\frac{k_1 l C_T}{\bar{v}_{zs}}$
Reaction parameter of CO_2 in the fiber	β_2	$\frac{k_1 l m [\mathrm{CO_2}]_{\mathrm{in}}}{\bar{v}_{zs}}$
Reaction parameter relative to the equilibrium	β_3	$4K_{\mathrm{eq}} m [\mathrm{CO_2}]_{\mathrm{in}}$
Arrhenius dimensionless number	γ_R	$\frac{E_R}{\Re T_l^0}$

$$p(\xi) = \frac{\varepsilon(\varepsilon+2) + 2\ln(1-\varepsilon)}{\varepsilon\{\varepsilon - 1 + (1-\varepsilon)\xi^2 - 2\ln\xi\}} \quad \text{(A10)}$$

and $\Omega_{CO_2} = \left[\Phi_{As}\Phi_{Bs} - \frac{(1-\Phi_{Bs})^2}{\beta_3\Phi_{Bs}}\right]$

subject to:

$$@\ \varsigma = 1, \quad \Phi_{As} = 1, \quad \Phi_{Bs} = 0 \quad \text{(A11)}$$

$$@\ \xi = \frac{r_o}{r_e} = \lambda_2, \quad \Phi_{As} = m\Phi_{Am}, \quad \text{and} \quad \left.\frac{\partial\Phi_{Bs}}{\partial\xi}\right|_{\xi=\lambda_2} = 0 \quad \text{(A12)}$$

$$@\ \xi = 1, \quad \left.\frac{\partial\Phi_{As}}{\partial\xi}\right|_{\xi=1} = 0, \quad \text{and} \quad \left.\frac{\partial\Phi_{Bs}}{\partial\xi}\right|_{\xi=1} = 0 \quad \text{(A13)}$$

The new dimensionless parameters derived are listed in Table 3.

Note that the dimensionless term $\frac{\bar{v}_{zs}d_o^2}{D_{As}l}$ is the Graetz number based on the external fibre diameter and the gas velocity in the shell side of the contactor.

The outlet mixing cup concentration rewritten in a dimensionless form is:

$$\Phi_{Afo} = 4\int_0^{\lambda_1} \xi(1-\xi^2)\Phi_{Af}\mathrm{d}\xi \text{ and}$$

$$\Phi_{Aso} = \frac{4(\phi-1)\int_{\lambda_2}^1 \xi\{(\varepsilon-1) + (1-\varepsilon)\xi^2 - 2\ln\xi\}\Phi_{As}d\xi}{(1-\varepsilon)(\phi-1)^2(\phi+1)^2 - 2\left[2\phi^2\ln\phi - \phi^2 + 1\right]}$$

$$\Phi_{Bso} = \frac{4(\phi-1)\int_{\lambda_2}^1 \xi\{(\varepsilon-1) + (1-\varepsilon)\xi^2 - 2\ln r\xi\}\Phi_{Bs}d\xi}{(1-\varepsilon)(\phi-1)^2(\phi+1)^2 - 2\left[2\phi^2\ln\phi - \phi^2 + 1\right]}$$

The extent of the soluble gas removal ψ which expresses the percentage of the solute in the gas stream that was recovered is defined as:

In the fiber bore $\psi_{CO_2,f} = \frac{[CO_2]_f^{in} - [CO_2]_f^{out}}{[CO_2]_f^{in}} = 1 - \Phi_{Afo}$ and, similarly in the shell, for the solute $\psi_{CO_2,s} = \frac{[CO_2]_s^{in} - [CO_2]_s^{out}}{[CO_2]_s^{in}} = 1 - \Phi_{Aso}$, and the solvent $\psi_{Am,s} = \frac{[Am]_s^{in} - [Am]_s^{out}}{[Am]_s^{in}} = 1 - \Phi_{Bso}$.